Chapter 1
Introduction

1.1 CYCLIC LOADING

Structural materials need to possess good mechanical properties along with resistance against corrosion and environmental degradation for their usage in various industrial applications. Majority of the structural components during their service undergo failures mostly due to cyclic loading (fatigue).Therefore, resistance of structural materials against low and high cycle fatigue, depending upon the service conditions, is very important.

During service, the nature of loading of engineering components and structures may change from symmetric to asymmetric condition. In symmetrical loading, the maximum and minimum stress levels in tension and compression are equal, whereas in asymmetrical loading the maximum and minimum stress levels are unequal. The classification of symmetrical and asymmetrical cyclic loading with analogous material response is depicted in Fig. 1.1.

Symmetrical cyclic loading may cause (i) failures occurring in the elastic region due to vibrations known as high cycle fatigue (HCF); (ii) failure occurring in the plastic region due to thermal gradients (during start up and shut down) known as low cycle fatigue (LCF).

Cyclic plastic deformation region, depending on the variation of cyclic load from symmetric to asymmetric, under stress/strain control modes can be classified as low cycle fatigue (symmetric strain controlled); mean stress relaxation (asymmetric strain controlled); ratcheting (asymmetric stress controlled). The main cause of premature failure of structures is cyclic plastic deformation. The component may not experience cyclic plastic deformation as a whole; however, there could be local stress concentrators such as defects and inclusions that cause failure.

Among various forms of cyclic plastic deformation, ratcheting fatigue has the maximum deleterious effect on fatigue life and hence has become subject of intense research [Paul, 2010a, 2010c, 2019].

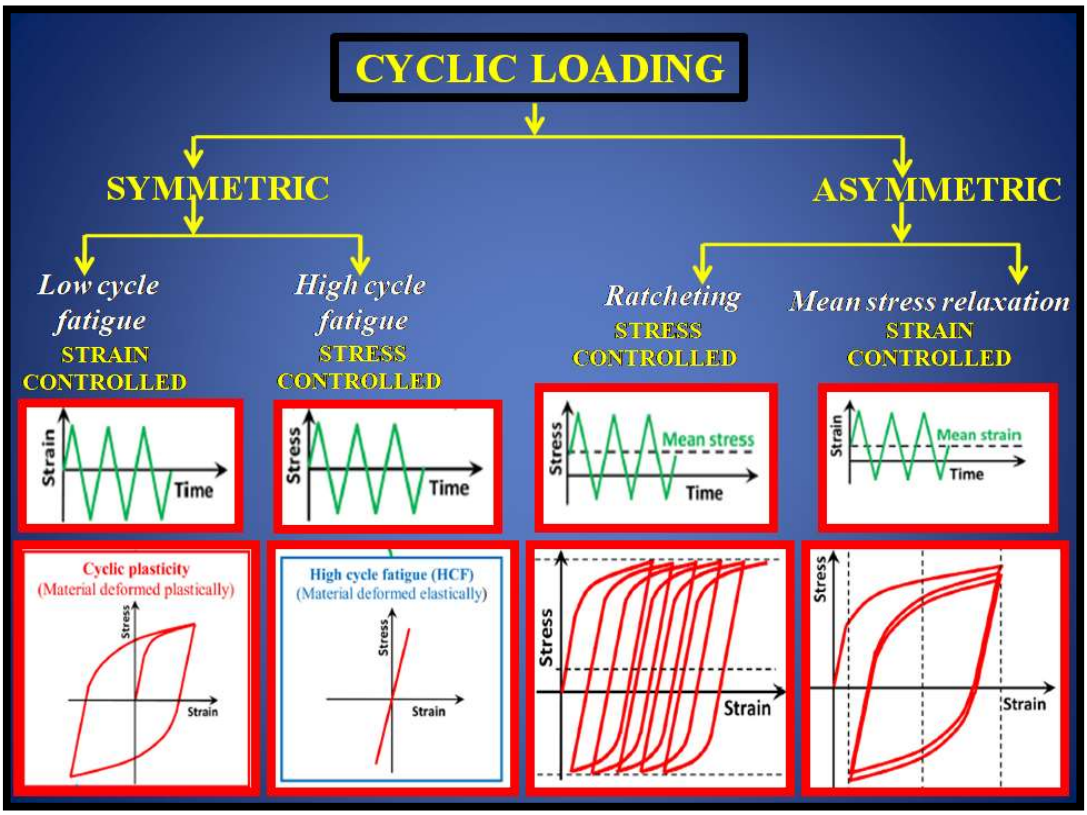

Fig. 1.1 Flow chart representing classification of cyclic loading with corresponding material behaviour [Paul, 2019].

1.2 RATCHETING

Ratcheting fatigue can be defined as progressive directional accumulation of inelastic strain. There is asymmetric stress controlled cyclic loading with mean stress in ratcheting fatigue, and the applied stress is high enough to cause yielding.

The phenomenon of ratcheting can be categorized as: (1) Material ratcheting, that is visible in a structure when the stresses are homogeneously distributed and (2) Structural ratcheting that occurs due to inhomogeneous multi-axial stress state.

The piping network comprising of straight pipes, curved elbows and tee joints are the most basic structures in primary heat transport system used in chemical, petroleum and power generating industries.

A simple example of structural ratcheting is a straight pipe experiencing a fixed internal pressure as well as cyclic thermal gradient. In this particular example, the primary load arises in axial and circumferential direction due to fixed internal pressure whereas secondary load (cyclic bending moment) occurs from cyclic thermal gradient. If the controlling loads are sufficiently high enough to deform the component plastically, structural ratcheting occurs and finally leads to collapse.

Contrarily in material ratcheting, strain accumulation occurs with number of cycles. It is a secondary deformation process, which severely deteriorates the performance of a component due to the additional effect of progressive directional inelastic strain accumulation and fatigue damage. It is purely material related effect, hence is observed during laboratory testing [Mukhopadhyay et al., 2014; Paul, 2019].

Ratcheting causes significant amount of plastic deformation in various engineering components and structures such as ovalization, reduction in cross-sectional area and bulging due to cyclic bending, internal pressure and cyclic loading. Due to these reasons, it is very essential to consider the phenomenon of ratcheting while designing the structure where structural integrity and safety are important. Otherwise, ratcheting can lead to catastrophic failure. Fig.1.2 displays final deformed shape of a pipe, resulting from ratcheting.

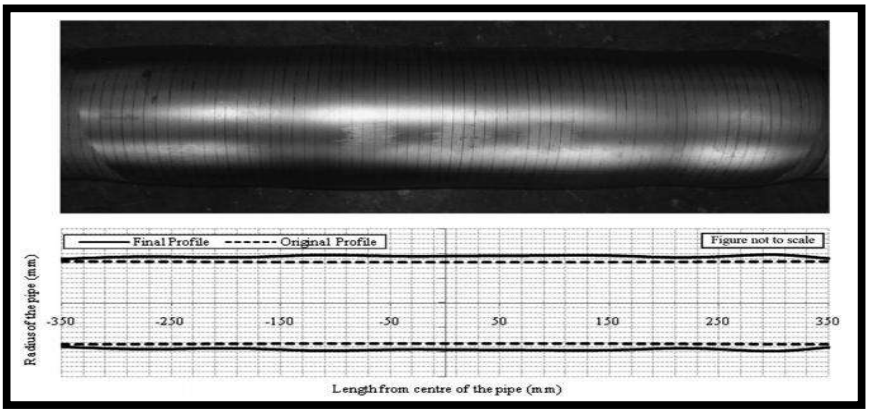

Fig. 1.2 The final deformed shape of pipe from ratcheting [Vishnuvardhan et al., 2010].

Ovalization and bulging can be observed when actual and final profiles of the pipe surfaces are compared [Paul et al., 2010b; Vishnuvardhan et al., 2010]. In ratcheting, deformation is caused due to combined effect of two processes, fatigue damage due to formation of cyclic hysteresis loops and directional accumulation of ratcheting strain, leading to severe deterioration or premature failure of the component.

1.3 RATCHETING STRAIN

Ratcheting strain is denoted by the centre location of the hysteresis loop, alongside the strain axis. It can also be considered as geometric mean of the peak and valley strain of that particular cycle

Mathematically, the axial ratcheting strain is expressed from cyclic stress-strain hysteresis loop as depicted in Fig. 1.3.

$$\epsilon_r = \frac{(\epsilon_{max} + \epsilon_{min})}{2} \tag{1.1}$$

where, ϵ_r = ratcheting strain

ϵ_{max} = maximum strain at a particular cycle

ϵ_{min} = minimum strain at the cycle.

Ratcheting strain is accumulated plastic strain under asymmetrical cyclic stressing whereas ratcheting strain rate is defined as cyclic increment of ratcheting strain per cycle. Ratcheting strain is influenced by many factors such as loading conditions, loading history, ambient temperature and loading path.

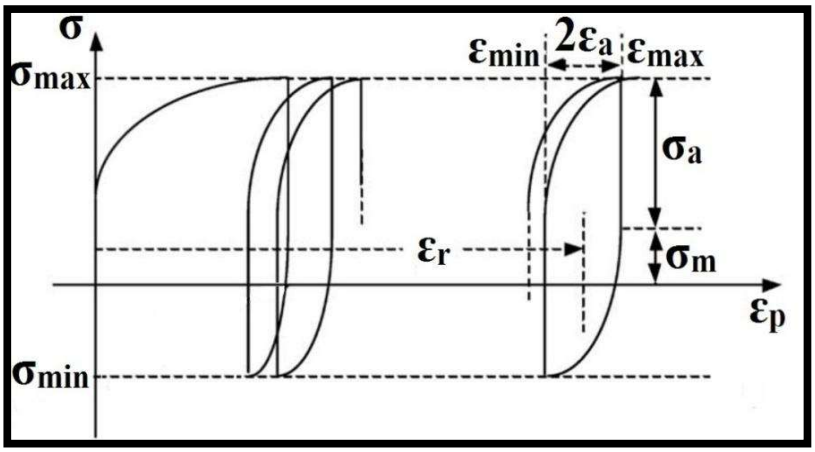

$(\sigma_a) = \frac{(\sigma_{max} - \sigma_{min})}{2}$ $(\sigma_m) = \frac{(\sigma_{max} + \sigma_{min})}{2}$

Fig. 1.3 Schematic representation of ratcheting fatigue [Gaudin & Feaugas, 2004].

Ratcheting strain and ratcheting strain rate curve with number of cycles for SA333 C-Mn steel, tested at a mean stress of 80 MPa and stress amplitude of 310 MPa, is depicted in Fig. 1.4(a and b). Analysis of the ratcheting strain curve reveals that ratcheting strain curve is very much similar to the creep curve having three zones; such as primary, secondary and tertiary. But the deformation mechanisms involved in both the phenomena are vastly different.

In the course of ratcheting experiments under engineering load/ stress control, two basic mechanisms are involved, geometrical softening and cyclic hardening of materials. In the primary region of the curve, cyclic hardening occurs because the reduction in cross- sectional area is small; hence the decay in ratcheting rate is basically due to

cyclic hardening. In the secondary region, there is a balance between cyclic hardening and reduction in cross-sectional area, thus steady state ratcheting is observed. In the tertiary region, due to very high accumulation of strain there is substantial decrease in cross-sectional area leading to softening of the material.

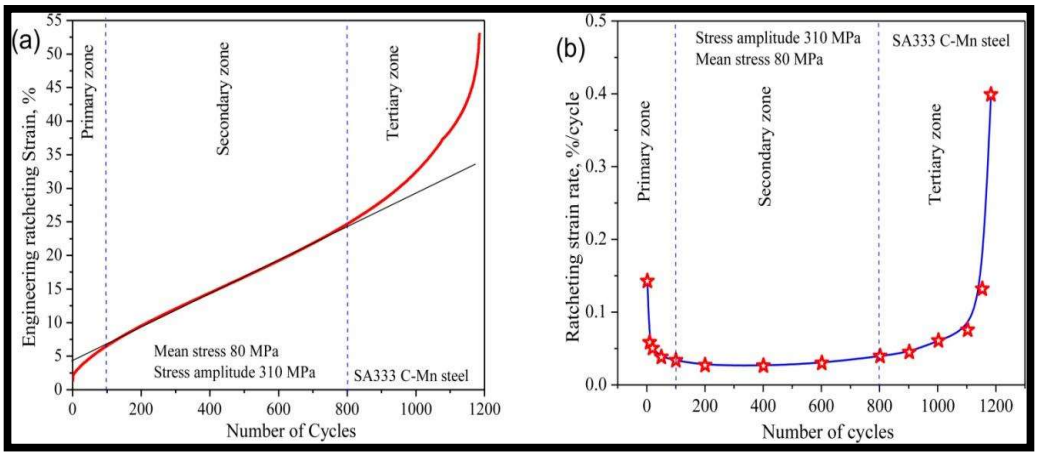

Fig. 1.4 (a)Variation of ratcheting strain with number of cycles (b) ratcheting strain rate curve exhibiting three zones for SA333 C-Mn steel tested at mean stress of 80 MPa and stress amplitude of 310 MPa [Paul et al., 2010c].

Ratcheting experiments can be conducted in two stress control modes: (i) engineering stress control mode and (ii) true stress control mode. Most of the research works available consider ratcheting under engineering stress control mode. If the ratcheting strain accumulation is quite low and there are no noticeable changes in specimen dimension then it is valid to consider engineering stress control mode. However, under cyclic loading with high magnitude of mean stress and amplitude, considerable alterations occur in specimen dimension and material fails by necking rather than fatigue crack initiation and propagation. Hence, from material point of view, it is necessary to characterize and model ratcheting response of materials under true stress control mode. On the other hand, from engineering application perspective, it is not

easy to measure and regulate true stress/strain during actual operation, thus engineering stress controlled experiments have gained much importance [Paul, 2011b ; 2019].

The advanced new generation power plants and industries use high temperature, pressure and aggressive environments to achieve higher efficiency and to reduce CO_2 emissions. Therefore, there is requirement of alloys of better performance to sustain such conditions. The alloy should possess superior mechanical properties, microstructural stability and resistance against oxidation and corrosion at elevated temperatures for long duration.

Modified 9Cr-1Mo steel and Inconel 617 alloys are used as piping and tubing material in various engineering components in power generating, chemical and petroleum industries. These alloys undergo different types of cyclic loading during their service and fail due to fatigue. This necessitates the study of ratcheting fatigue in these two alloys in the present investigation. Design, development, physical metallurgy, properties and applications of these two alloys are described in next section.

1.4 ALLOYS INVESTIGATED

1.4.1 MODIFIED 9Cr-1Mo STEEL

1.4.1(i) Development of Cr-Mo steels

Cr-Mo steels fall under the category of ferritic-martensitic steels. From last few decades, Cr-Mo steels have been primarily employed in advanced thermal and nuclear power plants, chemical and petroleum processing industries [Johnston et al., 1976] [Little & Stow, 1979]. In 1930s, when the requirement for creep resisitng steels was felt necessary, Cr-Mo steels were developed. It was observed that addition of 0.50% Mo to carbon steel, enhanced creep strength due to solid solution strengthening, but

exhibited poor ductility and was prone to graphitization. Futher, the Mo concentration was increased to 1% which eventually enhanced the creep strength and improved the ductility and also removed graphitization. Chromium content was further increased to preserve ductility and increase resistance against oxidation at elevated operating temperatures.

For applications up to 550–600°C, Mo concentration of 1% and chromium concentration of at least 2% was thought to be optimal for elevated temperature strength and oxidation resisstance respectively [Orr et al., 1978]. For use in more aggressive environments (e.g., in petrochemical and oil industry), alloys with higher chromium contents, such as 5Cr–12Mo, 7Cr–12Mo, 9Cr–1Mo, and 12Cr–1Mo, were introduced.

The hardenability of Cr-Mo steel increases by addition of more chromium (above 2¼%), and at a Cr content of 9%, the steel gets air hardened to fully martensitic structure in the commonly used section sizes. The resistance to oxidation and corrosion increases with increased Cr content. However, it was observed that with around 12% chromium content there was no significant enhancement in corrosion resistance [Orr et al., 1978; Babcock et al., 1971].

The new generation power plants have increased operating steam temperatures and pressures to achieve higher efficiency. This led to development of Modified 9Cr-1Mo steel (grade 91). This steel is modified version of the conventional 9Cr-1Mo steel (grade 9), which was modified by addition of carbide forming elements vanadium (V) and niobium (Nb), to enhance high temperature mechanical properties and microstructural stability [Klueh & Nelson, 2007]. These were further modified by substituting tungsten (W) and tantalum (Ta), as replacement to radiologically undesired

elements such as Mo and Nb. These steels are known as reduced activation ferritic martensitic (RAFM) steels.

1.4.1 (ii) Physical Metallurgy of Cr-Mo steels

Structural properties of any material are dependent on its microstructure and can be altered by specific heat treatments and alloying additions.

Significance of alloying elements in Modified 9Cr-1Mo steel

The effect of various alloying elements in modified 9Cr-1Mo steel is described below.

Cr–improves corrosion resistance and enhances mechanical properties by forming $Cr_{23}C_6$ precipitates.

Mo – acts as a solid solution strengthening element and retards dislocation recovery inhibiting the diffusion of Fe atoms. However, too much addition of Mo reduces the toughness by forming δ-ferrite and Laves phases (A_2B).

Nb –improves mechanical properties forming precipitates of carbides (NbC).

V– retards the growth of the carbide precipitates and also forms VC precipitates which improve mechanical properties. Nb and V were not there in Grade 9 steel. Due to presence of Nb and V in Grade 91 steel, there is good microstructural stability at high temperatures and improvement in creep resistance [Klueh, 1982].

C– exists in solid solution after solution treatment in the austenite phase field and precipitates as carbides during tempering treatment. Higher carbon content forms more number of carbides which easily coarsen during service and cause deleterious effect on creep resistance.

Ni and Mn – These are austenite stabilizers and are added to inhibit formation of δ –ferrite during austenitization.

Addition of Cr not only improves the corrosion resistance but also affects the resulting microstructure and mechanical properties. Cr and Mo are ferrite stabilizing elements.

Fig. 1.5(a) shows schematic pseudo-equilibrium phase diagram for the Fe-Cr-0.1%C system, it shows that the steel with 9% Cr may exist in one of several sub-liquidus phase fields depending on temperature [Sanderson, 1981]. At high temperature (> ~1473K) δ–ferrite + austenite; and from ~1473K to ~1073K austenite phase; at low temperatures ~1073K–1000K, there is α–ferrite (pro–eutectoid) + austenite+ primary carbides; and at low temperatures (< ~1000K) α–ferrite + primary carbides phases exist. The extent of any phase field present in a particular alloy depends on its composition.

In case of ferritic steels different microstructures (martensite, bainite, proeutectoid ferrite, or pearlite) can be produced by heat treatment, which have a substantial impact on their mechanical properties. The influence of a particular heat treatment is very well illustrated by an isothermal–transformation phase diagram or a continuous cooling transformation (CCT) phase diagram. For 9Cr–1Mo steel, CCT diagram (Fig. 1.5b) depicts that martensite can be formed at a wide range of cooling rates [Orr & Sanderson, 1984; Atkins,1978].

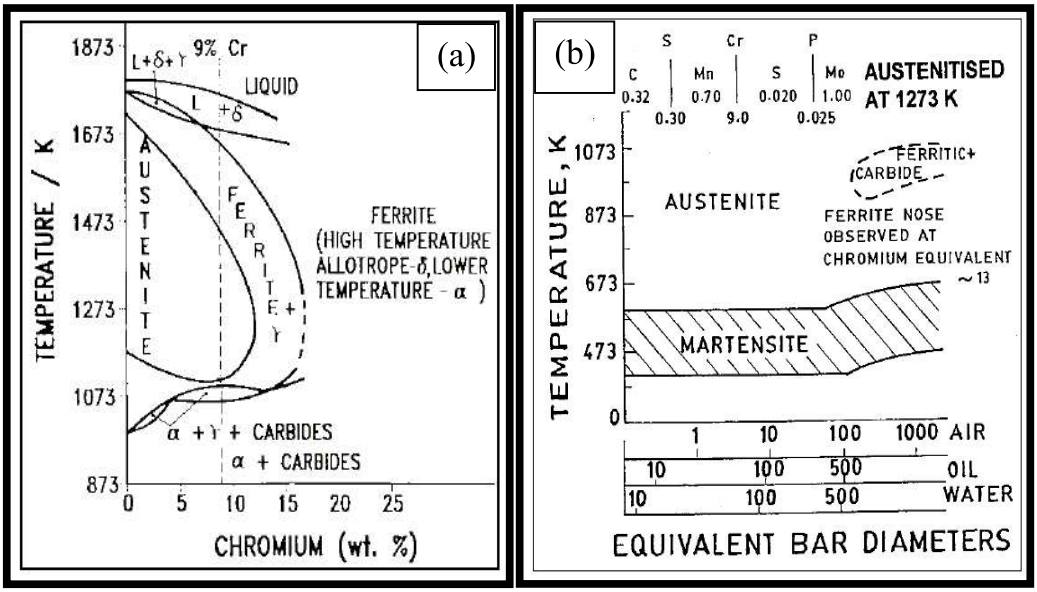

Fig. 1.5 (a) Schematic pseudo–equilibrium Fe (with 0.1%C)–Cr phase diagram [Irwine et al., 1960]. The dashed line indicates the phase fields for the steel with 9% Cr. (b) Continuous cooling transformation diagram for 9Cr–1Mo steel [Atkins, 1978].

Due to several alloying elements, 9Cr-1Mo steel has good hardenability. Among several heat treatments such as annealing, normalizing, and quenching, normalizing is preferred due to finer grain size than annealed microstructure, and less amount of residual stresses present as compared to those resulting from quenching. Tempering treatment is preferred after normalizing to relieve residual stresses. Impact toughness of the steel mainly depends on tempering temperature.

The optimum temperature for tempering is 740-820^{o}C. Even though the steel has good hardenability, some retained austenite (RA) can be found at martensite inter lath boundaries which is found to be mechanically stabilized by transformation stresses. Retained austenite transforms to untempered martensite upon cooling if the stressses are relieved to a certain degree by proper selection of tempering time and temperature. At lower tempering temperatures the stresses are relieved and RA transforms to untempered martensite, which is highly deleterious to toughness. At 750^{o}C elimination of transformation stresses and isothermal transformation of RA to ferrite proceeds simultaneously and also $Cr_{23}C_6$ carbide forms along PAGBs. As a result, no martensitic transformation occurs upon cooling [Shiue et al., 2000].

The optimum temperature range for normalizing is 1040-1100^{o}C. Higher normalizing temperatures are very deleterious to toughness owing to austenite grain coarsening [Chatterjee et al., 2014] and δ–ferrite formation [Kumar et al., 2003]. Thus, along with alloying additions heat treatment conditions also have considerable effect on microstructure and mechanical properties of Cr-Mo steels [Kim et al., 1999; Shrestha et al., 2015; Sikka, 1983].

The method of processing an alloy can be expected to affect high temperature fatigue properties, if different grain sizes and microstructures result as a consequence of

different processing procedures. As reported by Ebi1 & McEvily (1984), hot forged material exhibited inferior fatigue properties as compared to hot rolled material. Hot forging of alloy was done in the range of 1100-1150^{o}C and hot rolling at a lower range of temperature. In both the cases, microstructure consisted of tempered martensite structure and carbides, however, PAG size in case of the hot rolled condition was smaller (19 μm) than that of the hot forged condition (31μm). Coarse grains were found to be highly deleterious to fatigue life [Ebi1 & McEvily, 1984].

Pipings used in various components in power and chemical industries operate at high temperatures for long time periods which lead to change in microstructure and mechanical properties.Therefore, it is necessary to study microstructural stability of the modified 9Cr-1Mo steel. The microstructure of modified 9Cr-1Mo steel in normalized and tempered condition consists of lath martensite with very high dislocation density and precipitates of $M_{23}C_6$ and MX type carbides, generally found to be distributed along PAGBs, lath boundaries and inside the laths. The PAGs are of size nearly 20 μm [Paul et al., 2008; Verma et al., 2015]. The $M_{23}C_6$ precipitates have globular or lenticular morphology and size < 0.5 μm and are rich in Cr content, whereas MX particles are of size < 0.1 μm and are rich in vanadium and niobium.

In conventional 9Cr-1Mo steel, MX precipitates are not observed due to the absence of V and Nb. Thisis the reason that the conventional 9Cr-1Mo steel exhibits softening under creep test conditions at approximately 600^{o}C whereas the modified steel which contains V and Nb, exhibits superior stability and creep strength up to 704^{o}C. In general, the preferential nucleation sites for carbides are high energy regions like PAGBs and lath boundaries. PAGBs have high energy due to high degree of disorder at PAGBs than that of inter lath boundaries [Parida et al., 2013]. This is because adjacent

martensite laths have coherency with parent austenite grains and have good fit with each other whereas orientation relation between austenite grains can be random.

$M_{23}C_6$ (M: Cr, Fe) precipitates are found mostly distributed along PAGBs whereas MX ((V,Nb)(C,N)) are distributed in intra-lath regions. This is due to the fact that Cr has high diffusivity than that of V and Nb; therefore, even though PAGBs have high energy, V and Nb cannot diffuse to PAGBs and hence precipitates form within laths during tempering and increase creep strength by pinning down the moving dislocations, because of their fine size.

Thermal aging for long periods up to 10000 h at service temperatures of 550-650^{o}C leads to several changes in the microstructure of normalized and tempered modified 9Cr-1Mo steel such as coarsening of precipitates, annihilation and rearrangement of dislocations, leading to break up of martensite laths and gradual development of equiaxed sub structure and formation of A_2B type Laves phase [Jones et al., 1991; Paul et al., 2008].

During thermal aging two competitive processes occur, one is coarsening of precipitates and gradual break up of martensite lath structure leading to reduction in hardness and the other process is formation of Laves phases which leads to enhancement in hardness. Hence, due to these competing processes, there will be no observable change in hardness of steel after thermal aging for several hours [Jones et al., 1991].

It was reported that the growth of intra lath carbides, like MX type, is negligible as compared to that of $M_{23}C_6$ grain boundary carbides. This is because of low diffusivity of V and Nb, as compared to that of Cr. The growth rate of grain boundary carbides decreases after 5000 h due to the formation of Laves phases. These Laves phases form

like a shell, encapsulating $M_{23}C_6$ particles, which was confirmed by Paul et al. (2008) through X-ray elemental mapping.

These Laves phases are of the form A_2B with *hcp* crystal structure and rich in Fe and Mo. Extensive precipitation of these phases deprives the matrix of its Mo content which is detrimental to the strength of the steel. These phases are potential sites for crack initiation and make the steel susceptible to embrittlement. Formation of Laves phases can be avoided by employing high tempering temperatures for short time periods, to have more residual carbon in matrix.

1.4.1 (iii) Properties of modified 9Cr-1Mo Steel

1. Superior thermal conductivity
2. Low coefficient of thermal expansion compared to Austenitic Stainless Steels
3. Better creep and fatigue strength
4. Excellent neutron void swelling resistance
5. Excellent resistance to thermal stresses
6. Good hardenability

1.4.2 SUPERALLOY INCONEL 617

Superalloys are high-performance heat-resistant alloys with exceptional strength and oxidation resistance when exposed to high temperatures.These alloys can endure loads for long periods of time without mechanical degradation, even at service temperatures near the melting point of the alloys.In general, these alloys have a matrix of nickel, cobalt, or iron to which other alloying elements are added for strength. Solid solution strengthening is achieved by adding metals such as tungsten, molybdenum, tantalum, and niobium, whereas precipitation strengthening is achieved by adding elements such

as titanium and aluminium. These superalloys are preferred to other competitor materials such as ceramics and refractory metal alloys for high temperature applications because they have good mechanical properties, resistance to oxidation and corrosion, and microstructural stability at elevated temperature [Donachie & Donachie, 2002].

The emergence of many complex superalloys for aircraft and land-based applications was necessitated by the development of commercial gas turbine engines, and the diverse microstructural features of these alloys allowed the development of a wide range of alloys that can be optimised for specific applications through processing.Various researchers have produced and investigated a wide variety of superalloys intended for special applications.

The requirement of materials that can withstand high temperatures has propelled superalloy development to a high level of sophistication [Gasson, 2008]. Due to their high melting points, refractory metals can withstand high temperatures, but their poor oxidation resistance and ductility limit their use in many applications when compared to superalloys. Ceramic materials, despite their outstanding oxidation and corrosion resistance, have poor toughness and ductility,therefore do not match the requirements of the intended applications [Di Gianfrancesco, 2017].

Superalloys are divided into three categories based on the principal element contained in the alloys: 1. Iron-based superalloys, 2. Nickel-based superalloys and 3. Cobalt-based superalloys.The major classification of different superalloys along with several examples of commercially available superalloys is elaborated below.

1. **Iron-based superalloys**: The major constituent in iron-based superalloys is iron, with a minimum of 25% nickel content to stabilise the austenitic matrix. Addition of other alloying elements is to provide solid solution as well as

precipitation strengthening.These superalloys are less expensive than the other two categories of superalloys.

e.g. N-155, Haynes 556, 19-9 DL, Incoloy (800, 800H, 800HT, 801, 802).

2. **Nickel-based superalloys**: These superalloys contain nickel as major element. Other alloying elements such as Cr, Co, Mo, Al and Ti are also added to achieve the desired mechanical properties through solid solution as well as precipitation strengthening.

   e.g. Haynes (214, 230, HR-120, HR-160), Inconel (600, 601, 617, 625, 718) Hastelloy B, N, S, C-276, Nimonic alloy (80A, 90, 95).

3. **Cobalt-based superalloys**: The precipitation of carbides of refractory metals such as Mo and W along the grain boundaries strengthens these alloys.These are more expensive than nickel-based superalloys; thus, they are only utilised in crucial sections where the cost is justified [Tien, 2012].

   e.g. Haynes (25,188), Satellite B, UMCo-50, MP159.

1.4.2 (i) Nickel based superalloys

Nickel-based superalloys contain nickel as the main element for stabilising the austenitic (*fcc*) matrix and a combination of other alloying elements such as chromium (10-25%), cobalt (5-15%), molybdenum (~10%), aluminium and titanium (up to 8% combined) for improving high temperature properties. In some situations, tungsten and niobium are added to these alloys to give solution strengthening and carbide formation.Among the three groups of superalloys, Ni-based superalloys have a wide range of important applications, making them the most interesting alloys for metallurgists.These alloys were introduced in 1940 for use in jet engines where strong creep strength and stress rupture strength were required [Geddes et al., 2010]. As the

speed of jet engines increased, the working temperature of the engines was also raised, thereby the necessity for high heat resistant materials was also increased.

This led to the development of new nickel-based superalloys as well as the improvement of jet engine technology [Akca & Gürsel, 2015]. Depending on the fabrication method, superalloys can be polycrystalline, columnar grained, or single crystal. There is no universally accepted system for designating nickel-based superalloys. Nickel-based alloys comprise families of alloys under different designations such as Nimonic, Incoloy, Inconel, Hastelloy and Rene etc.

For many years, single crystal nickel-based superalloys have been used to make turbine blades. The first generation of superalloys were developed in the early 1950s [Akca & Gürsel, 2015] with the primary goal of boosting high temperature strength through the addition of γ' [$Ni_3(Ti, Al)$] formers, which reduce toxic phases and increase castability. Rhenium was not present in the initial generation of single crystal superalloys. This family of alloys includes CMSX-2 and Rene N4.

Single crystal super alloys of the second generation were introduced in the late 1980s and are commonly utilised in commercial and military aircraft engines. These alloys typically contain 3% rhenium (Re) by weight, which distinguishes them from single crystal super alloys of the first generation. The percentage of refractory element, Re, and γ' formers increased by more than 6% Rene N5, CMSX-4, and PWA 1484 are examples of second-generation alloys.

By raising Re addition to 6 wt% and reducing chromium content levels, third generation alloys were developed to boost temperature capacity and creep resistance even more. These alloys had Hafnium (Hf) in content. Rene N6, CMSX-10, and DMS4 are examples of these alloys.

Later, a fourth generation of superalloys emerged, containing platinum group metals, primarily Ruthenium (Ru). The EPM 102 alloy is an example of this generation, which has better phase stability and strength than the preceding alloys. EPM 102, a fourth-generation alloy, is around 6% heavier than second-generation alloys. Another example of this generation is TMS 138.

Due to the high alloy densities of later generation alloys, the application of superalloys was limited, and third and fourth generation alloys are now only used in specific applications. To obtain the necessary structure, the fifth generation of alloys included Ru more than 6 wt% as in TMS-162 and TMS-172. Two fifth-generation nickel-based single crystal super alloys, were developed in Japan in 2008. Both alloys were found to have high creep resistance. TMS-238 is a sixth-generation alloy produced by Japan's National Institute for Materials Science [NIMS]. The oxidation and hot corrosion resistance of the alloy were increased by lowering the Mo and W contents and increasing the Co and Ta contents [Prasad & Wanhill, 2017].

In nickel-based super alloys, there are four main primary phases [Jena & Chaturvedi, 1984]:

1. Gamma (γ)
2. Gamma Prime (γ')
3. Gamma double prime (γ'')
4. Carbides
5. Topologically close packed phases

1. **Gamma (γ)**: The matrix (also known as gamma) is a nickel-based austenitic phase with a face centred cubic (*fcc*) crystal structure. Co, Cr, Mo, and W are some of the elements that impart solid solution strengthening to the γ.

2. **Gamma Prime (γ')**: In these alloys, γ' is the main precipitation strengthening phase. In general, Ti or Al elements serve as γ' formers in the form of Ni_3Al or Ni_3Ti phases. These are coherent precipitates with a cube-on-cube orientation relation with the matrix. The crystal structure is an ordered *fcc* crystal structure.
3. **Gamma double prime (γ'')**: This phase is of Ni_3Nb having body centered tetragonal (*bct*) crystal structure and is coherent with the matrix (γ). In Ni-Fe alloys, this phase exists only in the presence of Nb and is unstable above 650^{o}C. This phase imparts high strength over a wide temperature range (450-750^{o}C).
4. **Carbides:** Carbon present in the range of 0.05-0.2 percent mixes with carbide-forming elements such as chromium, molybdenum, titanium, tantalum, and hafnium to produces carbides. During service or heat treatment, these carbides (MC) decompose to form other carbides such as $M_{23}C_6$ and M_6C at the grain boundaries.The carbides have the same crystal structure as that of the matrix (*fcc*).The development of carbides along grain boundaries increases the stress rupture strength of nickel-based superalloys at high temperatures.
5. **Topologically Close-Packed Phases (TCP):** Phases like σ, μ and Laves phases etc. form during heat treatment or service. They cause brittleness to these alloys making them undesirable. TCPs normally appear as plates at low magnification and as needles at high magnification. TCPs also have the negative impact of forming deleterious phases when they interact with γ and γ' phases, lowering the creep strength of the alloy [Sabol & Stickler, 1969].

1.4.2 (ii) Nickel-based superalloy Inconel 617

Inconel 617 a solid solution strengthened nickel base superalloy. In addition to Ni, the other alloying elements are Cr, Co and Mo. Solid solution strengthening is provided by the addition of Co and Mo whereas small amounts of Al and Ti impart precipitation

strengthening to the alloy. Strengthening is also induced by the formation of $M_{23}C_6$ and M_6C carbides. At high temperatures, there is formation of oxide layers of Cr and Al which makes this alloy resistant to oxidation and corrosion [Mankins et al., 1974].

Inconel 617 was developed in the year around 1970 and possesses better pitting and crevice corrosion resistance as well as excellent creep strength at temperatures beyond 850^{o}C [Hosier & Tillack, 1972]. It has good weldability and is metallurgically stable since it does not form harmful phases like σ, μ and χ at high temperatures. On comparing with other nickel-based alloys containing tungsten, this tungsten free alloy is less expensive and lighter. The alloy has good formability but requires large forming stresses because of the formation of carbides at elevated temperatures. The forging or hot working temperature range is around 1000 to 1200^{o}C for this alloy. Despite higher rate of work hardening, cold working can be carried out using conventional methods. After cold working, annealing at 1040^{o}C is essentially required for homogenizing the microstructure [Hosier & Tillack, 1972; Mankins et al., 1974].

Solution treatment is carried out for Inconel 617 alloy which results in a coarse grain structure that improves creep strength. At ambient temperature, this treatment offers the alloy its maximum strength and ductility. It also possesses high bend ductility at room temperature.

The solutionizing treatment cycle involves heating the alloy to 1175^{o}C and exposing it for a period of time, determined by the section size of the alloy, followed by quenching in water or quick cooling in air [Rao et al., 2019b].

1.4.2 (iii) Physical Metallurgy of Inconel 617 alloy

The phases that develop in Inconel 617 alloy are identical to those discussed previously, however, in the composition range indicated, no gamma double prime (γ'') and TCP phases form. The extra phase Ti(C, N) occurs during solidification or heat treatment, in this alloy, and is stable even at room temperature.

As reported by numerous researchers [Di Gianfrancesco, 2017; Kirchhöfer et al., 1984; Wu et al., 2008] phase transformation and phase stability in Inconel 617 alloy (subjected to aging treatment after solutionizing), can be elaborated with the aid of time temperature transformation (TTT) diagram.The TTT diagram for Inconel 617 alloy is depicted in Fig. 1.6 which provides information about the phases formed after aging treatment. Carbides and γ' are the two types of second phases that are formed in this alloy and may vary in proportion depending on the duration of the aging treatment.

Carbides: In Inconel 617 alloy, the reaction of various carbide forming elements with carbon produces three types of carbides: MC, M_6C, and $M_{23}C_6$, where M stands for carbide forming element (Cr, Mo, Co and Ti in this alloy). MC carbides occur during the solidification of the alloy and are largely heterogeneous or randomly distributed between grains and along grain boundaries, with no orientation relationship with the matrix. The crystal structure of MC is *fcc*. These carbides have script morphology and are often coarse in size. TiC is the most stable carbide at room temperature, present only in small amounts. Other MC carbides after heat treatment or processing, transform to $M_{23}C_6$ and M_6C carbides, this transition may happen during service as well.

During heat treatment or processing, M_6C carbides typically change from MC carbides in the temperature range of 815 to 980^{o}C. These are molybdenum-rich carbides, which take the form of $(Ni,Co)_3\ Mo_3C$. These carbides are useful for grain boundary

strengthening at high temperatures. These carbides have a complicated cubic structure and are stable at higher temperatures than those of $M_{23}C_6$ carbides.

$M_{23}C_6$ carbides, like $Cr_{23}C_6$, are chromium-rich carbides that develop at lower temperatures than M_6C carbides. These carbides are made of residual carbon in the solid solution or MC carbides that have been transformed. Since both have a *fcc* crystal structure, these carbides retain a cube on cube orientation relation with the matrix.$Cr_{23}C_6$ and $Cr_{21}Mo_2C_6$ are the two most common carbides.

Nickel or cobalt can substitute chromium to form complex carbides. These carbides are generally located near grain boundaries and hinder grain boundary sliding, increasing the creep rupture strength of this alloy at higher temperatures; thus, these carbides are essential phases in comparison to the other phases in this alloy. However, as these carbides emerge from the matrix due to decohesion under stressing, they act as nucleation sites for void formation, causing premature material failures that can be avoided by proper heat treatment.

Gamma prime (γ′): This phase has a *fcc* crystal structure and is an intermetallic phase compound. . This phase is commonly known as Ni_3(Ti, Al) phase and precipitates in the form of Ni_3Al or Ni_3Ti. This phase has a spherical morphology and is uniformly distributed throughout the matrix, although its volume fraction is quite low in this alloy due to the low concentration of Al and Ti.

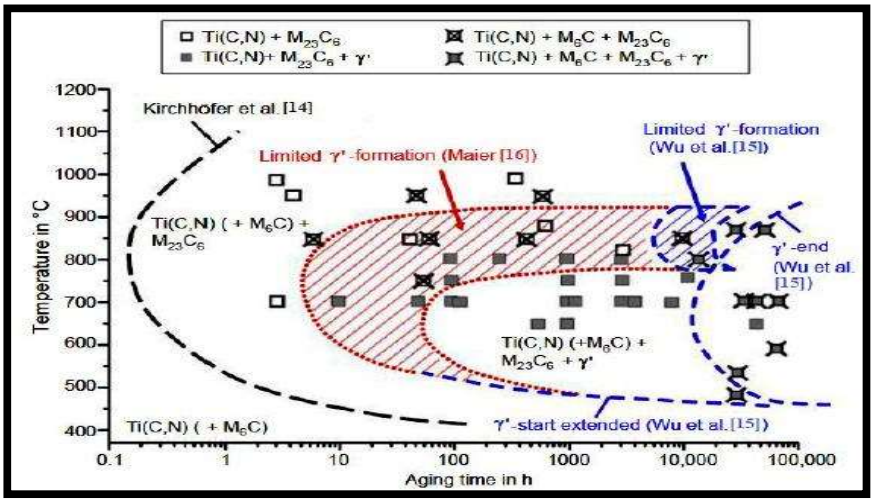

Fig. 1.6 TTT Diagram of Inconel 617 alloy showing temperature and time limits for formation of various phases [Di Gianfrancesco, 2017; Kirchhöfer et al., 1984; Maier, 2013; Wu et al., 2008].

1.4.2 (iv) Properties of Inconel 617 alloy

1. Excellent tensile and creep strength
2. High workability.
3. Good weldability.
4. Low co-efficient of thermal expansion
5. High thermal conductivity.
6. Low cost.
7. Good hardenability

1.5 APPLICATIONS

Both the alloys are used as piping and tubing material.

1. Used in advanced thermal and nuclear power plants in various engineering components such as: steam generator, superheater, reheater and heat exchanger.

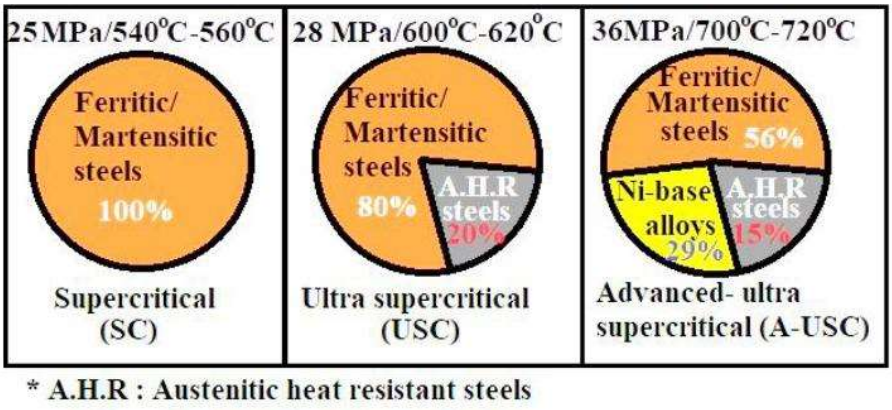

Fig. 1.7 The ratio of change in high temperature materials with steam parameters [Xie et al.,2015].

2. Used in chemical industries.
3. Used in oil and petroleum industries.
4. In metal processing.

1.6 Ratcheting behaviour of advanced structural materials

During the past three decades, the area of ratcheting fatigue has attracted the attention of numerous investigators. From 1990 to 2020, there is significant increase in the number of research articles and work in the field of ratcheting fatigue.

First investigation in the area of ratcheting was reported by Bairstow, (1911). Accumulation of plastic strain was observed in a steel specimen under uniaxial cyclic stressing with tensile mean stress.

Numerous other researchers also reported progression of axial strain under uniaxial asymmetric cyclic loading at elevated temperatures such as Kennedy, (1956); Lazan, (1950); Manjoine, (1949); Meleka & Evershed, (1960); at room temperature Benham & Ford, (1961); Coffin, (1960), and at low temperatures Moyar, (1960); Moyar & Sinclair, (1962); Bendler & wood, (1962).

Coffin Jr., (1964) observed shifting of cyclic stress-strain hystersis loops on deforming 1100 Aluminium, under cyclic stressing with mean stress. Later, Benham, (1961) performed substantial research on cyclic creep for mild steel. It was concluded that the rate of ratcheting depends on the hardening and/or softening behaviour of the material. Two forms of fracture were also observed, one was due to fatigue crack propagation and other was due to excesssive plastic deformation.

Radhakrishnan, (1975) carried out multiaxial ratcheting fatigue experiments on aluminium and steel. An alternate twist of ± θ between two tensile stressing increased the plastic strain on the following reloading.

Researchers focussed mainly on various aspects of ratcheting including various experimental aspects such as the influence of mean stress, stress amplitude, stress rate, path of loading, planar anisotropy, temperature, previous loading history. Ratcheting in engineering and true stress modes and their comparison has also been addressed. Ratcheting- tensile, ratcheting- LCF, ratcheting-creep and their life assessment has also been discussed.

During the last three decades, much of the research related to ratcheting fatigue is focussed on microstructural characterization and constitutive modelling related to ratcheting fatigue in various structural materials such as different grades of steels, alloys of aluminium, magnesium, zirconium and copper. In most of these studies, the effect of various parameters influencing ratcheting fatigue behaviour, modes of conducting ratcheting fatigue experiments and studies on ratcheting from specimen to component level are mentioned. Also the correlation of ratcheting fatigue with microstructural modifications, effect of ratcheting fatigue on other phenomenon such as

creep, tensile and low cycle fatigue, comparison of ratcheting fatigue behaviour of materials with different crystal structures are discussed.

1.6.1 Ratcheting at specimen level

1.6.1 (i) Effect of applied stress levels (mean stress and stress amplitude)

Dutta & Ray, (2013) conducted ratcheting fatigue experiments on interstitial free steel for 100 cycles with variation in mean stress at constant stress amplitude and change in stress amplitude at constant mean stress. Ratcheting strain was found to be increased with increase in mean stress from 10 MPa to 30 MPa at constant stress amplitudes of 130, 140 and 150 MPa as depicted in Fig. 1.8(a, b and c). The total ratcheting strain for all combinations of σ_m– σ_a is shown in Fig. 1.8(d) which illustrates that total ratcheting strain increases with increasing σ_a and σ_m level.

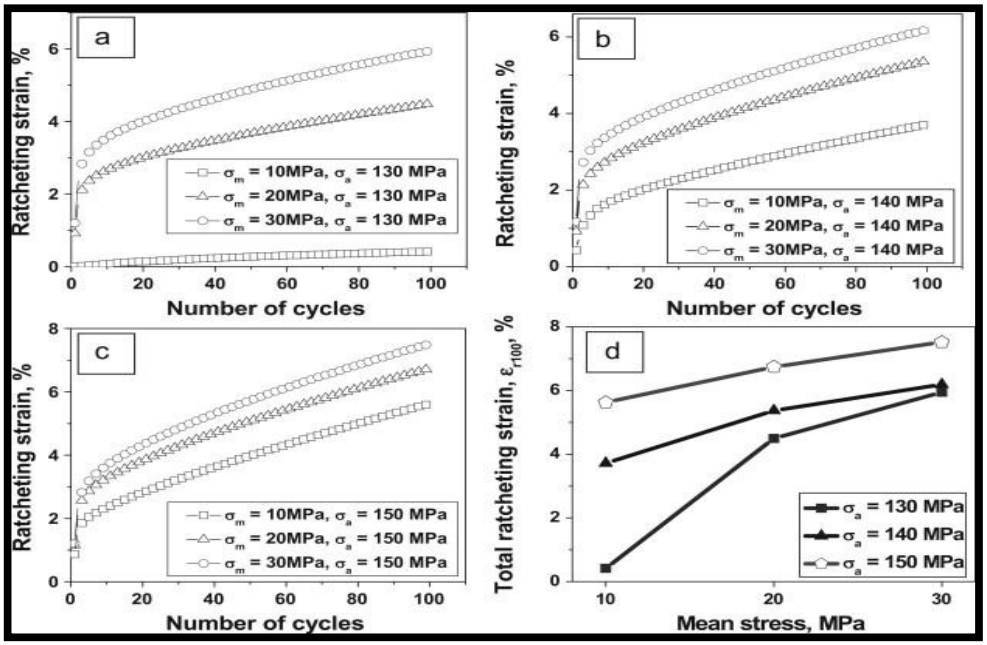

Fig. 1.8 Variation of ratcheting strain with increasing cycles for different mean stresses at different constant stress amplitudes of (a) 130 MPa, (b) 140 MPa, (c) 150 MPa, (d) accumulation of total ratcheting strain upto 100 loading cycles [Dutta & Ray, 2013].

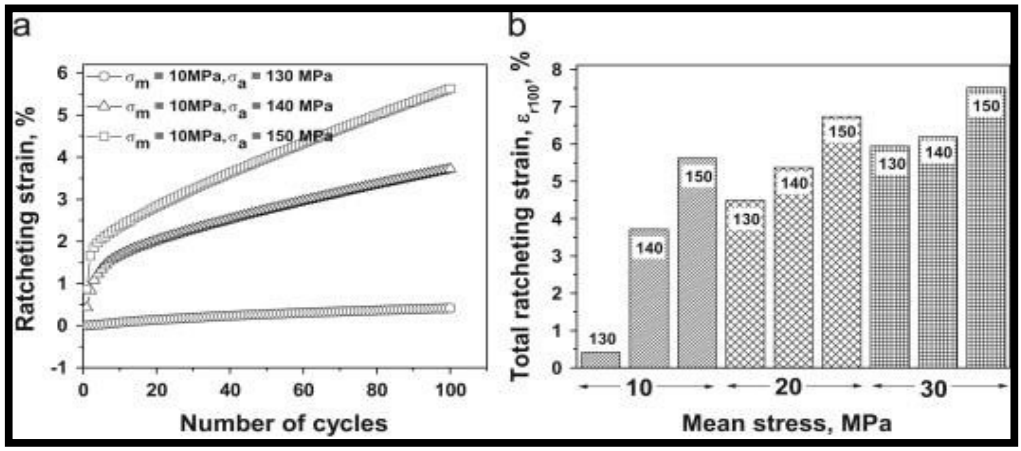

Fig. 1.9 (a)Variation of ratcheting strain with cycles at different stress amplitudes, at constant mean stress constant of 10 MPa. (b) bar chart shows total ratcheting strain upto 100 cycles of loading (values with the bars correspond to stress amplitudes in MPa) [Dutta & Ray, 2013].

Similar result was observed also with increase of stress amplitude. Ratcheting strain accumulation increases with rise in stress amplitude from 130 to 150 MPa at constant mean stress of 10 MPa as depicted in Fig. 1.9 (a). The total ratcheting strain upto 100 cycles of loading is shown by a bar chart in Fig. 1.9 (b).

For understanding the ratcheting behaviour, hysteresis loops generated during testing were analysed. Hysteresis loops for the tenth cycle at constant stress amplitude (σ_a) of 140 MPa and varying levels of mean stress (σ_m) from 10, 20 and 30 MPa are depicted in Fig. 1.10.

It was observed that for particular stress amplitude, with rise in mean stress, σ_{max} increased and that resulted in higher amount of plastic strain accumulation in the material; thus, plastic strain accumulation was increased with rise in mean stress values.

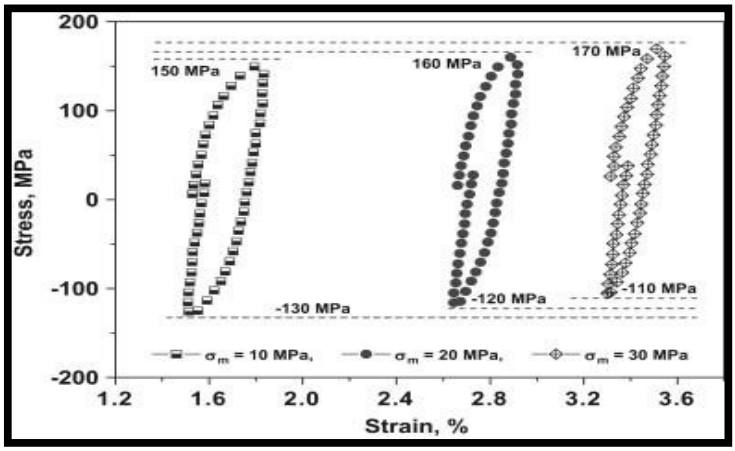

Fig. 1.10 Cyclic stress–strain hysteresis loops corresponding to 10^{th} cycle, at different mean stresses, depicting variations in their relative positions [Dutta & Ray, 2013].

Kong et al.,(2022) studied the uniaxial ratcheting fatigue behaviour and fracture mechanism of GH742 superalloy at 923K. The effect of mean stress and stress amplitude was analysed. It was found that with increase in mean stress and stress amplitude, there was reduction in fatigue life. Under asymmetrical loading, during initial cyclic stressing, the alloy showed cyclic hardening behaviour followed by cyclic softening upto fracture. Similar investigation was carried out by Liu et al., (2019) for nickel based superalloy GH4169 at 650^{o}C.

Similar results were observed with variation in mean stress and stress amplitude by Paul et al., (2011b, 2011a) for SA333 steel, Lim et al., (2009) for Cu alloy, Lin et al., (2013) for hot rolled AZ31B Mg alloy.

1.6.1 (ii) Influence of stress rate

Rajpurohit et al., (2016) studied ratcheting fatigue behaviour of Zircaloy-2 under various parameters, at ambient temperature. It was observed that with rise in stress rate,

accumulation of ratcheting strain decreases and there is enhancement in fatigue life of the material as displayed in Fig.1.11.

Wen et al., (2013) also studied the influence of stress rate on ratcheting fatigue of Zircaloy-4 tubes and reported similar result.

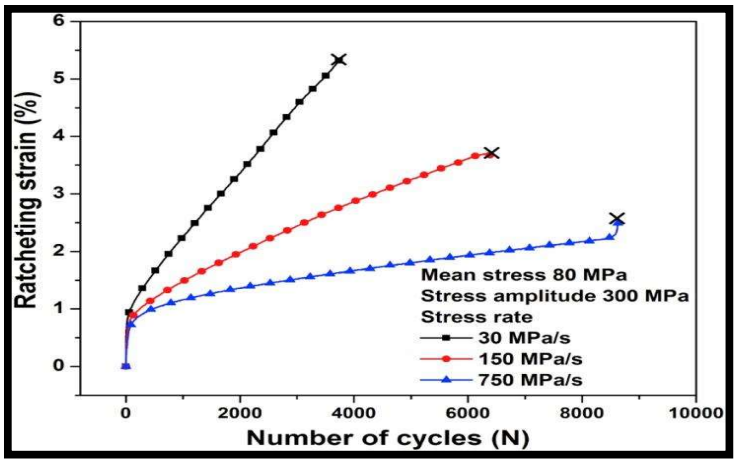

Fig. 1.11 Impact of stress rate on ratcheting fatigue of Zircaloy-2 displaying variation of ratcheting strain with cycles, at room temperature [Rajpurohit et al., 2016].

At 400^{o}C, opposite effect of stress rate was observed on the accumulation of ratcheting strain in Zircaloy- 2 by [Rajpurohit et al., 2018]. At the maximum stress rate of 750 MPa/s, there was reduction in plastic strain accumulation in comparison to that at 150 MPa/s, and that resulted in higher fatigue life. However, at the minimum stress rate of 30 MPa/s, it was found that accumulation of plastic strain was lower as compared to that at 150 MPa/s, as shown in Fig. 1.12. This behaviour was mainly attributed to the effect of dynamic strain aging (DSA) at 400^{o}C.

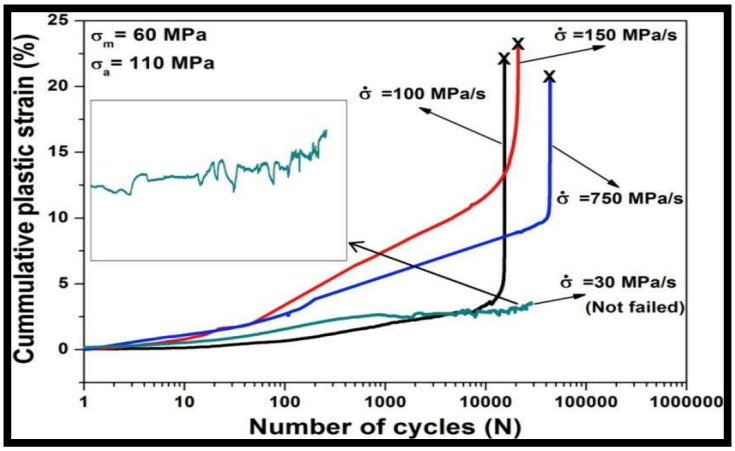

Fig. 1.12 Impact of stress rate on plastic strain build up with cycles at 400°C [Rajpurohit et al., 2018].

1.6.1 (iii) Influence of mean stress direction

Some investigators studied the effect of the direction of mean stress (tensile and compressive) on the accumulation of plastic strain Paul et al., (2011b, 2011a) performed two experiments on 304 LN stainless steel at the engineering stress amplitude of 420 MPa and engineering mean stress of + 60 MPa and -60 MPa. It was observed that ratcheting strain accumulation was higher in case of tensile mean stress as compared to the strain in the compressive mean stress as depicted in Fig. 1.13.

With increasing number of cycles, there was progressive accumulation of plastic strain in the direction of mean stress.Thus, in the case of tensile mean stress, true stress increased because the cross sectional area decreased due to the accumulation of tensile ratcheting strain. However, in the case of compressive mean stress, there was decrement in true stress as the cross sectional area of the specimen increased due to compressive ratcheting strain accumulation. In the case of tensile mean stress, true stress level increases whereas with compressive mean stress it gets lowered. Hence, the rate of ratcheting strain accumulation is higher for a specimen with tensile mean stress than

that of compressive mean stress. Similar observation was reported by Jiang & Sehitoglu, (1994) for the 1070 steel.

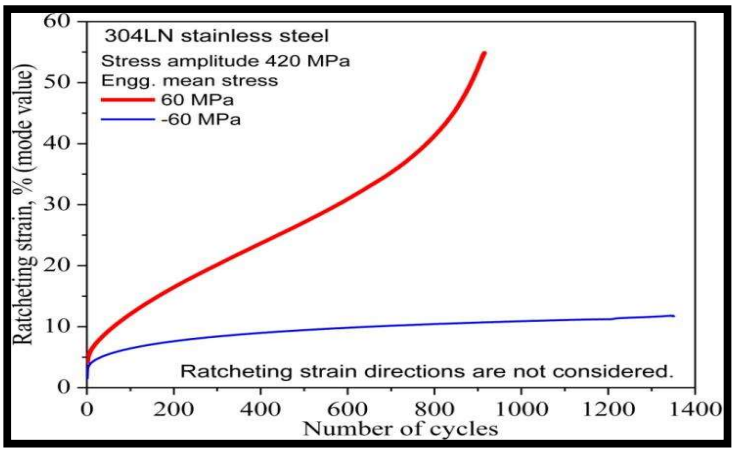

Fig. 1.13 Evolution of ratcheting strain with cycles for 304LN stainless steel at constant stress amplitude of 420 MPa and stress rate of 50 MPa/s [Paul et al., 2011b].

1.6.1 (iv) Effect of temperature

Temperature also plays a key role on evolution of ratcheting strain and fatigue life. Portier et al., (2000) reported that during multi-axial ratcheting on 316 austenitic stainless steel, there was enhancement in ratcheting strain accumulation with rise in temperature.

Rajpurohit et al., (2018, 2021) conducted ratcheting fatigue tests on Zircaloy-2 at ambient temperature, 300 and 400^{o}C. The results were compared, and it was found that with rise in test temperature, there was enhancement in fatigue life of the material (Fig. 1.14) and this was due to DSA in the temperature range of 300 to 400^{o}C.

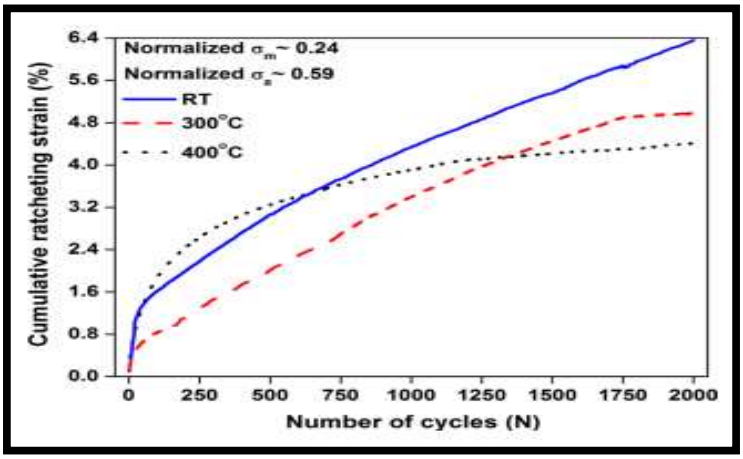

Fig. 1.14 Ratcheting strain accumulation at RT, 300, and 400 °C under normalized mean stress (σ_m/σ_{UTS}) and stress amplitude (σ_a/σ_{UTS}) in Zircaloy -2 [Rajpurohit et al., 2021].

1.6.1 (v) Effect of crystal structure

Kang et al., (2011) studied ratcheting fatigue behaviour of metals with different crystal structures and different values of fault energy by conducting cyclic stress controlled experiments at room temperature. The materials included were 316L stainless steel, pure copper, pure aluminium and ordinary 20# carbon steel. It was concluded that ratcheting behaviour not only depends upon the crystal structure or the fault energy, but is also influenced by the variation in mobility of dislocations. In case of polycrystalline materials, the generation of dislocations and their mobility is also effected by various microstructural features such as solute atoms, second phase particles, texture and grain boundaries.

The ratcheting behaviour is also dependent on the cyclic hardening/softening behaviour. In this investigation it was found that among three *fcc* metals, aluminium exhibited the most significant ratcheting behaviour (Fig. 1.15) because of its maximum fault energy and minimum cyclic hardening. In case of metals with different crystal structures, *bcc*

20# carbon steel showed more significant behaviour than *fcc* metals due to its cyclic stable features (Fig. 1.16).

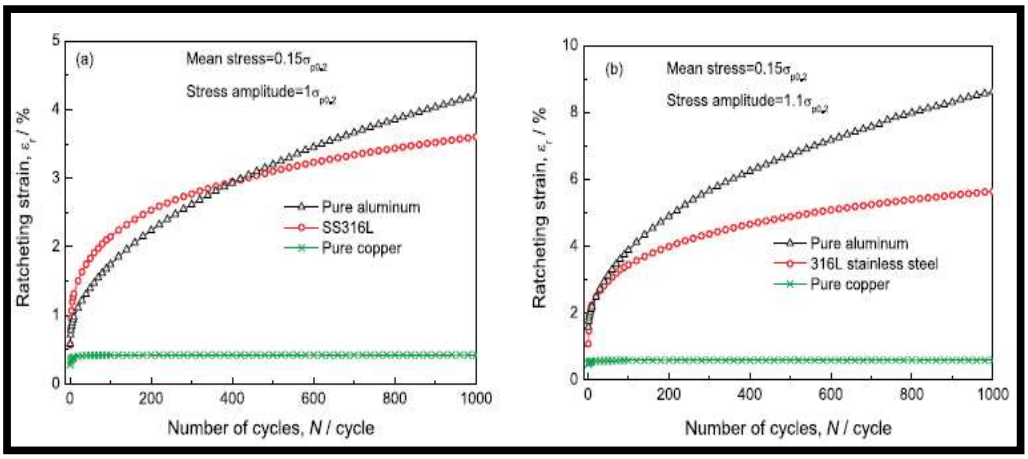

Fig. 1.15 Comparison of uniaxial ratcheting fatigue results of the prescribed *fcc* metals with different values of fault energy [Kang, Liu, et al., 2011].

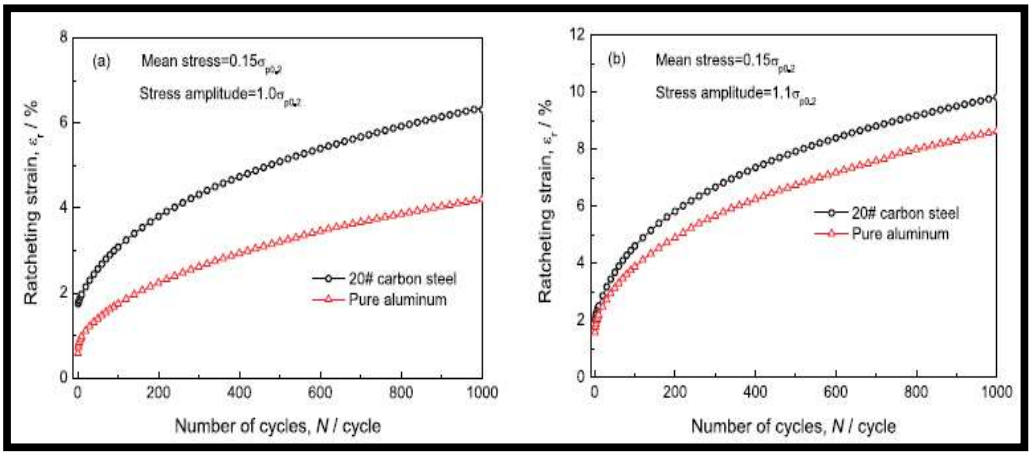

Fig. 1.16 Comparison of uniaxial ratcheting results for the prescribed metals with different crystal structures:(a) 0.15±1.0 σp0.2; (b) 0.15±1.1 σp0.2 [Kang, Liu, et al., 2011].

1.6.2 Modes of experimentation

Ratcheting fatigue experiments can be performed in two controlling modes: (1) engineering stress controlled mode (2) true stress controlled mode. Majority of

research on ratcheting fatigue has been carried out in engineering stress controlled mode because true stress/strain measurement and management are very difficult during service.Thus from the application point of view, engineering stress controlled ratcheting experiments are more relevant. True stress controlled tests, are required to characterize and model the ratcheting fatigue response of materials.

From comparison of the two modes, it is very clear that in case of true stress controlled testing, correction of cross-sectional area comes into picture and consequently the applied loads are corrected. In engineering stress controlled mode, no such corrections are incorporated in the applied load. Paul et al., (2010c, 2011b) performed experiments in the two modes on SA333C-Mn steel. It was observed that there was improvement in fatigue life in true stress controlled mode in comparison to that in the engineering stress controlled mode, as depicted in Fig. 1.17.

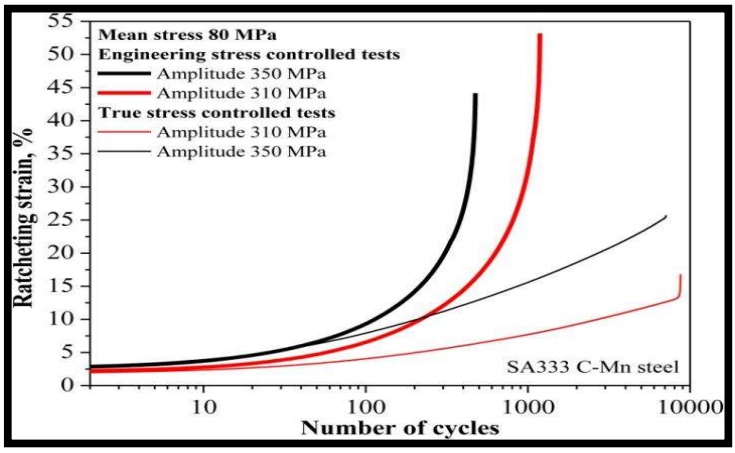

Fig. 1.17 Comparison of ratcheting fatigue of the SA333C-Mn steel under true and engineering stress control at a mean stress of 80 MPa and stress amplitudes of 310 and 350 MPa [Paul et al., 2010c].

The reason behind the reduction in fatigue life during engineering stress controlled testing may be attributed to (a) rapid accumulation of plastic strain; (b) rise in the level of true stress; (c) instability and necking due to reduction in cross sectional area. In true

stress controlled mode, failure occurs by initiation and propagation of fatigue cracks. It may be clearly observed from Fig. 1.17 that during initial cycles under the two modes, accumulation of plastic strain is almost equal. With increase in the number of cycles, there is variation in ratcheting strain build up.

1.6.3 Effect of ratcheting on mechanical behaviour

Dutta & Ray, (2013) performed ratcheting tests on IF steel for 100 cycles of loading. There after, the same specimens were tested under tensile loading. It was observed that both yield as well as tensile strength of the ratcheted sample was found to be higher in comparison with those of the unratcheted sample. The enhancement in yield strength was almost 110% from the preratcheting whereas the increase in tensile strength was only about 15% (Fig. 1.18). This can be very well correlated with the width of cyclic stress- strain hysteresis loops.

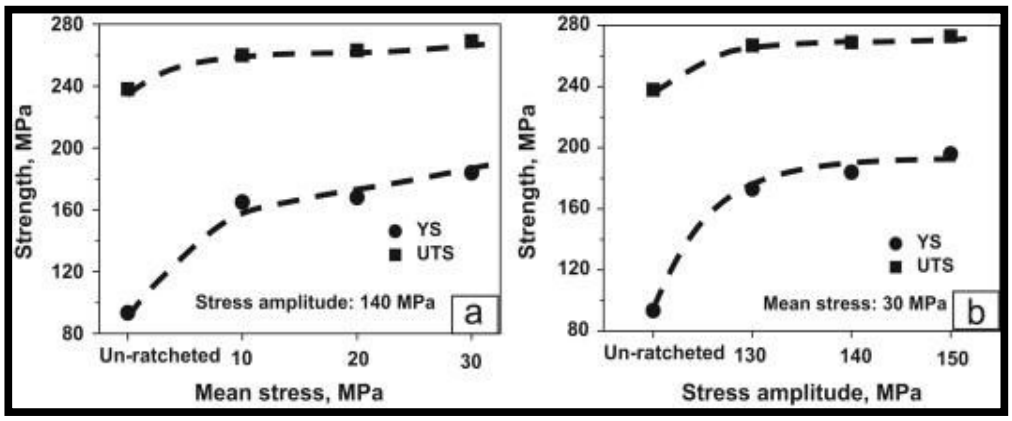

Fig. 1.18 Comparison of yield strength and ultimate tensile strength of the un-ratcheted and ratcheted specimens of the investigated IF steel: (a) at constant stress amplitude and varying mean stresses, (b) at constant mean stress and varying stress amplitudes [Dutta & Ray, 2013].

With increase in the number of cycles, the width of the hysteresis loops decreased as depicted in Fig. 1.19, which is an indication of cyclic hardening of the material. The

strength parameters of the ratcheted samples increased as a result of cyclic hardening of the IF steel.

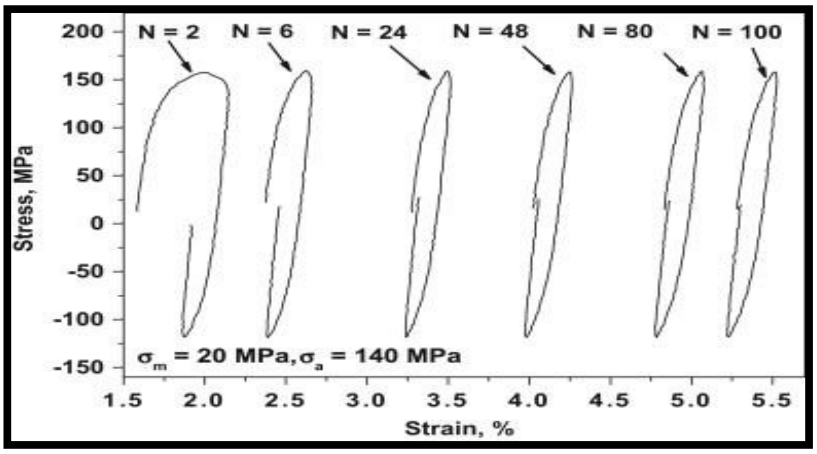

Fig. 1.19 Variations in the width of hysteresis loops showing cyclic hardening phenomenon for the investigated IF steel [Dutta & Ray, 2013].

Ando et al., (2012) reported the effect of ratchet strain on fatigue and creep-fatigue strength of modified 9Cr-1Mo steel. The influence of ratcheting deformation on failure cycles was studied by conducting uniaxial fatigue and creep-fatigue tests with superimposed strain at different temperatures. In fatigue tests at 550^{o}C, it was observed that there is reduction in cyclic life with superimposed strain in comparison with the tests without imposition of strain. It was also concluded that all the number of cycles with superimposed strain was within a factor of 1.5 of those of without superimposed strain. Inversely, the failure life increased due to build up strain at 450^{o}C. The accumulated stain was insignificant in creep–fatigue tests with superimposed strain, according to test results. As long as the parameters are within the strain limits of the design and construction code for fast reactors, the influence of ratcheting deformation on fatigue and creep–fatigue life was considered insignificant.

1.6.4 Microstructural characterization

Initially the research on ratcheting fatigue behaviour has emerged with the aid of macroscopic experimentation and constitutive modelling. These models are totally based on the macroscopic experimentation and are unable to provide a precise simulation of accumulation of ratcheting strain for the materials with different cyclic hardening/softening features, various loading histories, and complex multiaxial loading paths. Hence, it becomes very important to understand the microstructural evolution (micro-mechanisms) in ratcheting.

Microstructural investigations on different materials have been carried out by various researchers such as [Gaudin & Feaugas, 2004; Kang et al., 2010, 2014; Kang, et al., 2011; Dong et al., 2012, 2013 ; Sarkar et al., 2013 ; K Dutta et al., 2010; Krishna Dutta & Ray, 2013; Rajpurohit et al., 2016, 2018].

Dutta & Ray, (2013) conducted ratcheting studies on IF steel with tensile mean stress. Since the loading is asymmetric in nature the number of dislocations generated during loading cycles will be higher than that during unloading cycles. However, in the course of load reversal only the fraction of dislocations that are generated gets annihiliated. As a result, a significant amount of dislocations persist as residuals in the substructure of steel.

It is commonly known fact that higher the remnant dislocation density, more is the plastic strain accumulation and vice-versa. Thus, it is implied that with rise in σ_m for a specific σ_a, the total strain accumulation increases due to an increase in remnant dislocation density. Fig. 1.20 depicts the variation in dislocation density at constant σ_m of 30 MPa, at varying stress amplitudes of 140 MPa and150 MPa

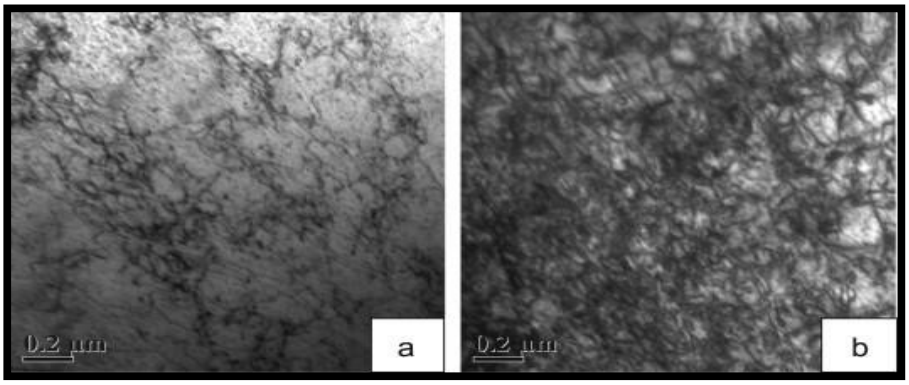

Fig. 1.20 Dislocation density variation under cyclic stressing at σ_m = 30 MPa: (a) at σ_a =140 MPa, (b) at σ_a =150 MPa [Dutta & Ray, 2013].

Kang et al., (2011) have performed uniaxial ratcheting behaviour of ordinary 20 carbon steel (*bcc*) macroscopically and microscopically at room temperature. It was reported that there is development of dislocation patterns from low density modes (dislocation lines and networks) to high density modes (dislocation tangles, walls, and cells) with number of cycles during low cycle fatigue and ratcheting. In case of ratcheting, there is formation of sub grains due to re-arrangement of dislocations.

1.6.5 Ratcheting at component level

Study of ratcheting fatigue is extremely essential while designing of mechanical parts such as pipelines of thermal/nuclear power plants, railways,turbine rotors and chemical industriesthat are exposed to thermo-mechanical cyclic loading. In pipelines, internal fluid pressure serves as mean stress in addition to it, cyclic loading can be generated due to variation in fluid pressure, temperature or seismic events. Experiments are required under component level (full scale) as well as specimen level to fully comprehend the ratcheting phenomenon.

Kulkarni et al., (2003) performed ratcheting tests on SA333Gr.6 carbon steel pipe with steady internal pressure and repeated bending load. It was observed that evolution of ratcheting strain occurs in the circumferential direction whereas there was no build up of ratcheting strain in the longitudinal direction. Yahiaoui et al., (1996) conducted ratcheting fatigue studies on long and short radius elbows made of carbon and stainless steels, under steady internal pressure and cyclic in-plane bending. It was reported that build up of plastic strain is higher in the crown hoop direction than in the axial direction.

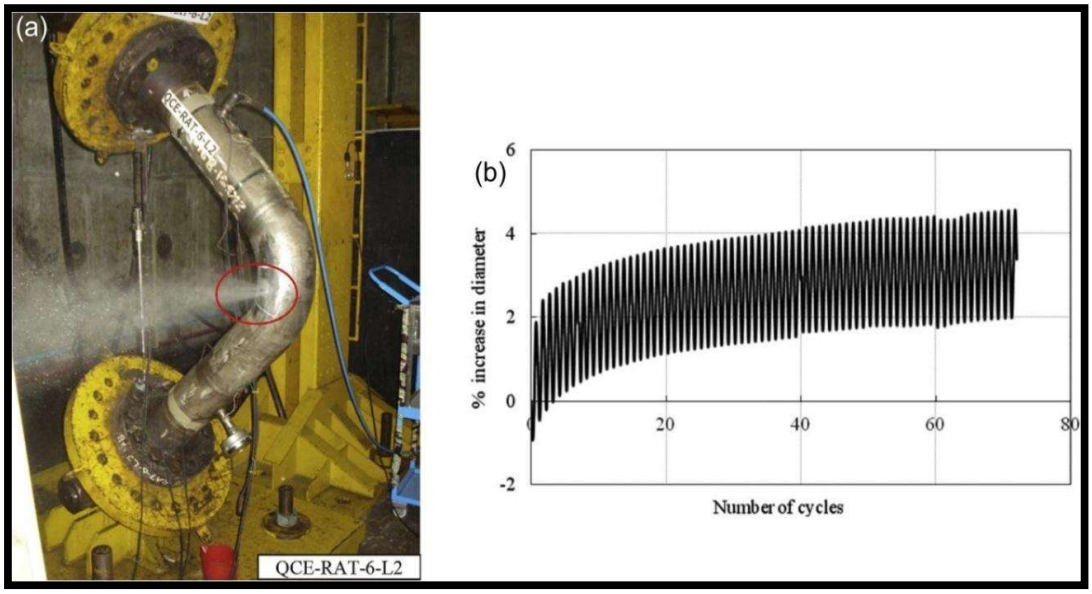

Fig. 1.21 (a) Occurrence of through-wall crack indicated by a sharp water jet: ratcheting experiment conducted with internal pressure of 39.2 MPa and displacement of ± 41 mm i.e. maximum load range ± 272 kN, (b) Percentage increase in diameter vs. number of cycles during ratcheting test on the elbow specimen with internal pressure of 37.9 MPa and displacement of ± 51 mm i.e. maximum load range ± 309 kN [Vishnuvardhan et al., 2013].

Vishnuvardhan et al., (2013) carried out ratcheting experiments on four elbows and four straight pipes, exposed to constant internal pressure and cyclic bending load, and observed that failure was due to axial through wall crack, followed by simultaneous

ballooning and thinning. Fig. 1.21(a) depicts detection of wall crack by spiky water jet and Fig. 1.21(b) shows percentage increase in diameter against number of cycles.

Currently various investigations have been explored in different aspects of ratcheting as well as on different classes of materials. Dwivedi et al., (2022) performed texture analysis on HSLA steel under asymmetric cyclic loading. Dutta et al., (2021) analysed the role of characteristic dislocations in controlling ratcheting and creep-ratcheting behaviour of a 356 Al-alloy. Cheng et al., (2021) studied ratcheting fatigue behaviour of unidirectional off – axis composites along with modelling and characterization. Zhang et al., (2022) observed molecular sources of ratcheting in poly-dispersed polycarbonate. Chen et al., (2022) analysed ratcheting behaviour of SA305 solders used for electronic packaging, with the aid of model.

1.7 MOTIVATION FOR THIS WORK

Several studies have been conducted on tensile properties, low cycle fatigue, creep fatigue interaction, corrosion and aging behaviour of the modified 9 Cr-1Mo steel [Baek et al., 2009; Jung & Kim, 2019; Kannan et al., 2011; Verma et al., 2015, 2016] and Inconel 617 alloy [Guo et al., 2013; Lei et al., 2021; Rao et al., 2019a, 2019b; Totemeier & Tian, 2007]. However, ratcheting fatigue behaviour of these alloys has not been explored; therefore, the present investigation is performed to characterize the behaviour of modified 9Cr-1Mo steel and Inconel 617 alloy under asymmetric cyclic loading, at room and elevated temperatures under various parameters.

1.8 OBJECTIVES OF THE PRESENT INVESTIGATION

1. Ratcheting fatigue behaviour of modified 9Cr-1Mo steel and Inconel 617 alloy at RT under three parameters mean stress, stress amplitude and stress rate (σ_m, σ_a and $\dot{\sigma}$) along with deformation and fracture behaviour in detail.
2. Ratcheting fatigue behaviour of modified 9Cr-1Mo steel and Inconel 617 alloy under mean stress effect at their respective service temperatures of 600^{o}C and 800^o C, with their microstructural and factrographic features.
3. Ratcheting fatigue behaviour of these alloys at 0.42 T_m homologous temperature along with their deformation and fracture behaviour.
4. Influence of ratcheting fatigue, resulting from mean stress, stress amplitude and stress rate (σ_m, σ_a and $\dot{\sigma}$) on tensile properties of modified 9Cr-1Mo steel and Inconel 617 alloy, at ambient and high temperature along with their deformation and fracture behaviour.